ANALYSIS AND DESIGN OF AN UHF RFID METAL TAG USING MAGNETIC COMPOSITE MATERIAL AS SUBSTRATE

S.-K. Kuo

Iron and Steel Research and Development Department
China Steel Corporation
81233 Kaohsiung, Taiwan

J.-Y. Hsu and Y.-H. Hung

New Material Research and Development Department
China Steel Corporation
81233 Kaohsiung, Taiwan

Abstract—Using magnetic composite material as the substrate for RFID metal tag has several advantages over conventional metal tags, such as flexibility and miniaturized size. In this paper, the radiation intensity contributed by a half-wave dipole is derived based on the result of an ideal Hertzian dipole, which leads to a simple relation for thin substrate. Later on, the material constants of two materials are measured and the one capable of generating greater radiation intensity is used in the course of antenna design. A primitive pattern design demonstrates the metal tag has a satisfactory 2.7 m reading range, and a dimension of $80 \times 22 \times 2 \, \text{mm}^3$.

1. INTRODUCTION

Since the destructive interference of electromagnetic waves offered by metallic surface poses a significant challenge for RFID tag design, only few stories had been reported by steel industries in the past years [1, 2]. Commercial RFID tags for tagging metallic items can be divided into two categories. The first kind has a sandwich type structure, in which a dielectric layer is placed between the antenna pattern and the metal ground [3, 4]. Due to its considerable price, the

metal tag has limited applications where recycling can be accomplished after the usage process. The other kind of the tag appears in the form of smart label, which uses special antenna design principles to avoid metal interference. For instance, the Flag Tag manufactured by UPM Rafsec lifts the RFID tag in the air by fixing the tag onto a vertical "flap" [5]. For another example, due to the unique radiation pattern offered by the monopole antenna, the smart label design reported by Kuo et al. has impressive performance when placed on the inner surface of the steel coils [6]. Even though these designs can be commercially available at very competitive prices to support one-time-use applications, they are applied in very few circumstances where high profile is not an issue.

A new appearance of the RFID tag was reported by Yang et al., which integrates the tag antenna with the magnetic composite material made by filling up polymer with magnetic particles [7]. By exploiting the flexibility of the polymer, as well as the permeability offered by the magnetic inclusions, a miniaturized RFID tag is designed to place upon surfaces with considerable curvature, such as plastic bottles and human wrist. The use of magnetic composite for substrate of RFID tag opens up opportunities for solving metal interference problem. Because most of the wave absorbers are made up of magnetic composite materials, using wave absorber to avoid destructive interference from the metallic items receives much attention recently. However, the mechanism provided by the wave absorber that helps the metal tag alleviating the interference problem has never been investigated. This paper presents the analysis and design of the RFID metal tag using the magnetic composite material. In Section 2, a relationship between the radiation intensity and the material property is established, which is later validated by simulation results. The measurement of electromagnetic properties of the magnetic composite is discussed in Section 3. In Section 4, a dipole type RFID metal tag design using the measured material constants is presented. Conclusions are drawn in Section 5.

2. ANALYSIS OF RADIATION INTENSITY

In most applications, having an extensive read range is the primary consideration in the design of the RFID metal tags. Therefore, the influence of the radiation intensity imposed by the wave absorber must be fully investigated. The discussions in this section extend the previous result of Hertzian dipole towards the real half-wave dipole, which provides a general rule for choosing better materials when designing metal tag antennas.
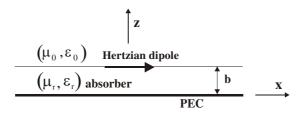
Figure 1. A Hertzian dipole on a grounded magnetic composite material.

2.1. Radiation Intensity of a Hertzian Dipole

Figure 1 shows a Hertzian dipole on top of a grounded wave absorber characterized by material parameters (μ_r, ε_r). The radiation pattern is given by [8]

$$E_\phi = I\Delta x \sin\phi \left(\frac{j\omega\mu_0}{4\pi r}\right) e^{-jk_0 r} F(\theta) \tag{1}$$

$$E_\theta = -I\Delta x \cos\phi \left(\frac{j\omega\mu_0}{4\pi r}\right) e^{-jk_0 r} G(\theta) \tag{2}$$

$$F(\theta) = \frac{2\tan(\beta_1 b)}{\tan(\beta_1 b) - j\dfrac{N(\theta)}{\mu_r}\sec\theta} \tag{3}$$

$$G(\theta) = \frac{2\tan(\beta_1 b)\cos\theta}{\tan(\beta_1 b) - j\dfrac{\varepsilon_r}{N(\theta)}\sec\theta} \tag{4}$$

in which $\beta_1 = k_0 N(\theta)$, $N(\theta) = \sqrt{\mu_r\varepsilon_r - \sin^2\theta}$.

In most cases, since the RFID reader is always arranged in front of the metal tag during the interrogation process, only $\theta = 0°$ is considered. Therefore, (3) and (4) becomes,

$$F = G = \frac{2Z_f}{Z_f - jZ_0} \tag{5}$$

with

$$Z_f = Z_0 \sqrt{\frac{\mu_r}{\varepsilon_r}} \tan\left(\frac{2\pi}{\lambda_0}\sqrt{\mu_r\varepsilon_r}\,b\right) \tag{6}$$

It is observed that the Z_f in (6) is exactly the impedance of the wave absorber. Equation (5) indicates maximum field intensity can be obtained when $Z_f = jZ_0$ is realized, yielding the condition

$$\sqrt{\frac{\mu_r}{\varepsilon_r}} \tan\left(\frac{2\pi}{\lambda_0}\sqrt{\mu_r\varepsilon_r}\,b\right) = j \tag{7}$$

Suppose at 925 MHz the equivalent thickness of the substrate is 2 mm, and fix the parameter $\varepsilon_r = 1$, solving (7) iteratively yields $\mu_r = j25.8$. Such a property can only be realized by artificial metamaterial due to the positive imaginary permeability [9, 10]. There are mainly two difficulties in design and implementation of such metamaterials. The first one is related to the cell size, which should be large enough to create resonance at nearly 1 GHz. The second one is the limited bandwidth provided by such structure. Using natural substances such as magnetic material is another way to realize antenna substrates for better radiation intensity and elevated bandwidth. Therefore, it is important to study how the electromagnetic properties of the material affect the performance of an antenna.

2.2. Radiation Intensity of a Half-wave Dipole

In real cases since the antenna has maximum radiation intensity when its size approaches half wavelength, the current on the antenna has sinusoidal distribution, $I(x) = I_0 \cos(\frac{2\pi x}{\lambda_g})$, where I_0 is the amplitude of the oscillating current, and λ_g is the guided wavelength. The electric field strength contributed by an infinitesimal current $I(x)\,dx$ becomes,

$$dE_\phi = I_0 \cos\left(\frac{2\pi x}{\lambda_g}\right) \sin\phi \left(\frac{j\omega\mu_0}{4\pi\,r}\right) e^{-jk_0r} F dx \tag{8}$$

$$dE_\theta = -I_0 \cos\left(\frac{2\pi x}{\lambda_g}\right) \cos\phi \left(\frac{j\omega\mu_0}{4\pi r}\right) e^{-jk_0r} F dx \tag{9}$$

The total field is given by integrating (8) and (9) over the half wavelength of the guided wave along the conducting strip on the grounded absorber,

$$E_\phi = \frac{\lambda_g}{\pi} I_0 \sin\phi \left(\frac{j\omega\mu_0}{4\pi r}\right) e^{-jk_0r} F \tag{10}$$

$$E_\theta = -\frac{\lambda_g}{\pi} I_0 \cos\phi \left(\frac{j\omega\mu_0}{4\pi r}\right) e^{-jk_0r} F \tag{11}$$

The radiation intensity is given by

$$U = \frac{r^2}{2Z_0} \left(|E_\phi|^2 + |E_\theta|^2\right) = \frac{1}{2Z_0} I_0^2 \left(\frac{\lambda_g}{\pi}\right)^2 \left(\frac{\omega\mu_0}{4\pi}\right)^2 |F|^2 \tag{12}$$

Since the guided wavelength is different from the wavelength inside the absorber by a correction of material constant [11],

$$\varepsilon_{eff} = \frac{\varepsilon_r + 1}{2} + \frac{\varepsilon_r - 1}{2} \frac{1}{\sqrt{1 + 6H/W}} \tag{13}$$

where H and W are the thickness of the absorber and width of the conductor. Generally speaking, the design of the metal tag usually requires a low profile feature (small H) and a large antenna gain (large W), i.e., $H \ll W$. In such way, the guided wavelength λ_g is approximately equal to the wavelength of the absorber, i.e., $\frac{\lambda_0}{\sqrt{\mu_r \varepsilon_r}}$. By suppressing constant terms in (12), radiation intensity is expressed as

$$U = C \cdot \left| \frac{2 \dfrac{1}{\sqrt{\mu_r \varepsilon_r}} Z_f}{Z_f - j Z_0} \right|^2 \tag{14}$$

Assuming the effective thickness of the absorber $\sqrt{\mu_r \varepsilon_r} b$ is small comparable to quarter wavelength, first order approximation $\tan(x) = x$ is adopted to generate the following result,

$$U \cong C \left| \frac{4\pi}{\lambda_0} \sqrt{\frac{\mu_r}{\varepsilon_r}} b \right|^2 \tag{15}$$

which indicates the ratio μ_r / ε_r plays an important role in determining the read range of a metal tag.

2.3. Simulation Results

In order to verify the conclusion reached in Section 2.2, simulations are performed using HFSS. A model is constructed by placing a half-wave dipole on a substrate with grounded surface, as depicted in Fig. 2. The dipole is excited by a constant current (1 amp), showing a sinusoidal current distribution along the dipole length. Two sets of simulation results are presented. Table 1 lists the simulation result of the first set, which comprises three cases with equal μ_r to ε_r ratio. As predicted by (14), all cases having the same μ_r / ε_r value generates the same field strength, while the last one has the smallest antenna size due to its high material constants. The second set has different μ_r / ε_r ratios, as indicated in Table 2. It is seen the agreement is not perfect for the case of $(\mu_r, \varepsilon_r) = (4, 1)$, which might be due to numerical simulation errors and fringing effects at both ends of the dipole, as well as the uncorrected guided wavelength. As a reference, theoretical predictions calculated using (14) are also listed in Tables 1 and 2. As a rule of thumb, choosing substrate material with larger μ_r / ε_r values will definitely increase the reading range.

Figure 2. HFSS model of a half-wave dipole.

Table 1. Simulated radiation intensity with the same μ_r/ε_r ratio.

(μ_r, ε_r)	Antenna size (mm)	Simulated U (milli-Watt)	Calculated U using (14) (milli-Watt)
(1, 1)	162.16	183.52	216.2
(2, 2)	81.08	207.40	216.2
(3, 3)	54.05	200.93	216.2

Table 2. Simulated radiation intensity with different ratios of μ_r/ε_r.

(μ_r, ε_r)	Antenna size (mm)	Simulated U (milli-Watt)	Calculated U using (14) (milli-Watt)
(1, 4)	81.08	59.01	54.0
(2, 4)	57.33	104.04	108.1
(1, 2)	114.66	118.35	108.1
(4, 1)	81.08	591.3	864.7

3. MEASUREMENT OF MATERIAL ELECTROMAGNETIC CONSTANTS

Many wave absorbers are commercially available on the market, covering a wide range of frequency distribution. In order to evaluate the feasibility of using such absorbers as the metal tag substrate, a 1 mm-thick absorber, AB5100, manufactured by 3M is considered.

The material constants are measured by a set of coaxial probes and calibration kits as seen in Fig. 3. Material parameters are calculated by processing the scattering parameters S_{11} and S_{12} using the Nicholson-Ross-Weir (NRW) algorithm [12, 13], which demonstrates a very high permittivity value over the measurement range as observed in Fig. 4. In order to validate the measurement accuracy provided by the coaxial probe, a comparison between the attenuation disclosed in the datasheet and the calculation result using the measured constants is performed. As depicted in Fig. 5, the two results shows a pretty matched agreement. The attenuation reaches a maximum at 2 GHz, which is quite close to the UHF range. However, using AB5100 as the metal tag substrate is unable to achieve satisfactory read range due to the following reasons.

The design of the wave absorber requires the impedance of the absorber Z_f expressed in (6) to be matched with the free space intrinsic impedance Z_0, i.e., $Z_f = Z_0$ [13]. Since most wave absorbers are made
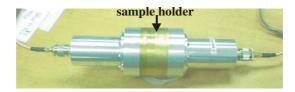

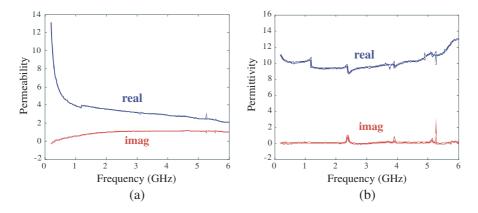**Figure 3.** Measurement of material constants using coaxial probe system.

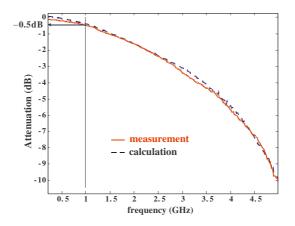**Figure 4.** Measured material constants of CIP wave absorber. (a) Permeability, (b) Permittivity.

Figure 5. Attenuation of magnetic composite material made by carbonyl iron powder.

by thin substrate, i.e., $b \ll \lambda_0$, filling the polymer with inclusions of high material constants becomes the only way to reach the matching condition. Due to the limited bandwidth offered by the magnetic materials, doping high permittivity substance when manufacturing the wave absorber is a common approach to achieve high material constants. However, substrate with high permittivity constant cannot produce satisfactory read range as the permittivity ε_r appears in the denominator of both (13) and (14). Conclusively, the traditional wave absorbers that achieve satisfactory wave attenuation results cannot be used here as the substrate of the metal tags.

Because of its unique micro structures, Carbonyl iron powder (CIP)is noted for its excellent microwave feature at GHz range [15]. To this end, a homemade absorber was manufactured by mixing proper weight percentage of carbonyl iron powder and silicon polymer. The measured material constants depicted in Fig. 6 demonstrate its superior characteristics for the metal tag design. The permeability shown in Fig. 4(a) drops rapidly at low frequencies, and then decays very slowly above 500 MHz. On the other hand, a much lower permittivity over a wide frequency range can be observed in Fig. 4(b). Even though the material exhibits a rather poor wave attenuation performance of 0.5 dB at 1 GHz as seen in Fig. 5, the radiation intensity according to (14) is about 3.2 times (5.1 dB) larger than 3M's sample.

4. DESIGN OF THE ANTENNA PATTERN

Because of its material properties, designing antenna pattern for the wave absorber requires special considerations. A dipole type antenna is proposed in this section, which includes a matching network to attain perfect impedance matching. The optimization of the antenna dimensions can be divided into two stages. In the first stage, dipole length is chosen based on the trade-off between the antenna gain and the impedance matching considerations. In the second stage, the dimension of the matching circuit is adjusted to achieve perfect matching condition.

4.1. Dipole Length Determination

The two stages of the design process can be explained using Fig. 6. The dipole length L_n is swept linearly across a wide range so as to search for its maximum antenna gain as seen in Fig. 7, which is found to be -4.6 dBi at $L_n = 29$ mm. The impedance trace (trace 1) of the L_n sweep on the Smith Chart is also shown in Fig. 8, which has a behavior similar to a lossy transmission line because of the decaying radius. The energy dissipating feature comes from the small imaginary constants as illustrated in Fig. 4. Even though $L_n = 29$ mm has the largest antenna gain, the location on the Smith Chart makes it difficult to attain impedance matching with the chip. Choosing L_n as 26 mm sacrifices antenna gain by only 0.7 dB; however, better impedance matching can be accomplished as explained in the Section 4.2. The overall performance can be enhanced by a slightly decreased gain but a much superior matching condition. As depicted in Fig. 7(b), the radiation pattern is similar to a patch antenna, having a 3 dB beamwidth around 100 deg.
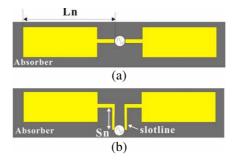

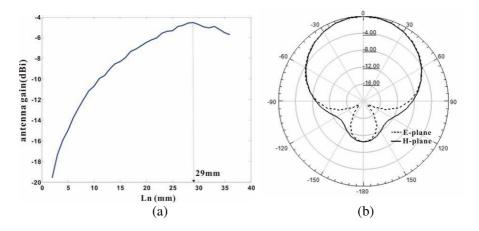**Figure 6.** Antenna design process. (a) The 1st stage, (b) the 2nd stage.

Figure 7. Determination of L_n. (a) Antenna gain variation by sweeping L_n, (b) radiation pattern of $L_n = 26\,\text{mm}$.
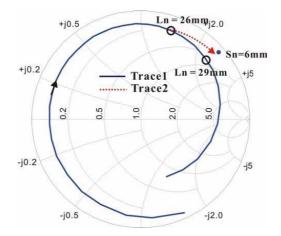

Figure 8. Impedance matching process using Smith Chart.

4.2. Adding Matching Network

In the next stage, a transmission line S_n is added to the antenna as shown in Fig. 6(b). By increasing S_n, the trace (trace 2) on the Smith Chart rotates clockwise until it reaches the conjugate of the chip impedance, as seen in Fig. 8. Instead of using a microstrip line, the transmission line is realized by a slotline because the energy inside the microstrip line decays faster due to the lossy characteristics of the material. Eventually, an impedance of $24 + j127\,\Omega$ is achieved

so as to meet the chip impedance $11 - j131\,\Omega$. In order to verify the performance of the impedance matching, the technique of using differential probe for accurate impedance measurement is adopted [16]. Similar to the RFID strap, the differential probe as seen in Fig. 9(a) can provide balanced feed that exerts currents with equal amplitude to the antenna. For a balanced antenna having a symmetric structure, i.e., $Z_a = Z_b$ in Fig. 9(b), the impedance converted by the differential signal S_{dd11} becomes,

$$Z_{dd11} = \frac{2Z_a Z_c}{2Z_a + Z_c} \qquad (16)$$

which is exactly the impedance "seen" by the RFID chip. The antenna has an impedance measurement value of $24 + j128\,\Omega$, quite close to the simulation result. A very attractive feature offered by the absorber based metal tag is its wide bandwidth. The most infamous feature of the low profile UHF metal tags is their narrow bandwidth, which usually ranges from 15 to 25 MHz [17]. Patch antennas using substrates loaded with magnetic films are known to have larger bandwidth [18, 19]. Using wave absorber can also increase the bandwidth for metal tags because of its magnetic property. The return loss of the antenna can be calculated from the measured antenna impedance Z_{dd11} and the chip impedance Z_{chip}, using

$$\Gamma = \frac{\left| Z_{dd11} - Z_{chip}^* \right|}{\left| Z_{dd11} + Z_{chip} \right|} \qquad (17)$$

The impedance bandwidth shown in Fig. 10 indicates the design has a 3 dB bandwidth of 100 MHz, which covers the whole UHF range.
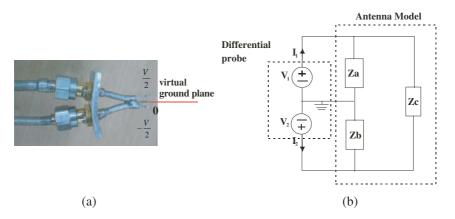

Figure 9. Adjusting the antenna impedance using the differential probe. (a) Differential probe, (b) the antenna is considered as a two-port π-network.
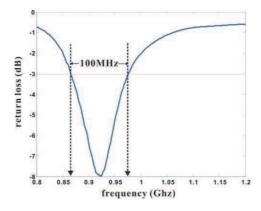
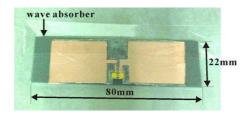**Figure 10.** Measured impedance bandwidth of the metal tag.

Figure 11. Metal tag design using magnetic composite material.

4.3. Reading Range Test

The prototype of the metal tag as shown in Fig. 11 has a miniature size of $80 \times 22 \times 2\,\text{mm}^3$. Since the radiation pattern depicted in Fig. 7(b), is similar to a patch antenna, the size of the metal should be large enough to prevent radiation on the back side. A reading range test using a 6 dBi circularly polarized antenna and 30 dBm reader power demonstrates the tag has 2.7 m reading range while placed on a 12 cm square aluminum plate. It decays to 2.1 m when the plate size is reduced to 9 cm. The calculated antenna efficiency is around 10%, while the efficiency is 45% for another metal tag design with more extensive reading range over 6 meters [17]. The degraded antenna efficiency is primarily due to the lossy characteristics of the absorber, which dissipates a portion of the energy by its nonzero imaginary material constants.

5. CONCLUSIONS

The effect of the magnetic composite material on metal tag applications is different from its original wave attenuation purpose, as the excitation

source of the former one is a half-wave dipole, while the latter one is simply a plane wave. Analysis result shows that better radiation intensity can be achieved by choosing material with higher permeability to permittivity ratio, which is later confirmed by simulation results. Further measurement of material constants reveals that due to excessive permittivity values, a commercially available wave absorber is not an appropriate substrate when extensive reading range is desired. Based on the measured material constants, a metal tag is designed and fabricated based on composite material fill up with carbonyl iron powder, which demonstrates a 2.7 m read range with 2 mm thickness and miniature size.

REFERENCES

1. Chen, S.-L., S.-K. Kuo, and C.-T. Lin, "A metallic RFID tag design for steel-bar and wire-rod management application in the steel industry," *Progress In Electromagnetics Research*, Vol. 91, 195–212, 2009.

2. "ThyssenKrupp steel's success with RFID noted," RFIDNews, Sep. 7, 2007.

3. Eunni, M. B., "A novel planar microstrip antenna design for UHF RFID," M.S. Thesis, University of Kansas, Jul. 2006.

4. Mo, L., H. Zhang, and H. Zhou, "Broadband UHF RFID tag antenna with a pair of U slots mountable on metallic objects," *Electronics Letters*, Vol. 44, No. 20, 1173–1174, Sep. 2008.

5. European Patent Application, EP1632926.

6. Kuo, S.-K., S.-L. Chen, and C.-T. Lin, "Design and development of RFID label for steel coil," *IEEE Transactions on Industrial Electronics*, Vol. 57, No. 6, 2180–2186, Jun. 2010.

7. Yang, L., L. Martin, D. Staiculescu, C. P. Wong, and M. M. Tentzeris, "A novel flexible magnetic composite material for RFID, wearable RF and bio-monitoring applications," *Procs. of the IEEE-IMS Symposium*, 963–966, Atlanta, GA, Jun. 2008.

8. Jackson, D. R. and N. G. Alexopoulos, "Simple approximate formulas for input resistance, bandwidth, and efficiency of a resonant rectangular patch," *IEEE Transactions on Antennas and Propagation*, Vol. 39, No. 3, Mar. 1991.

9. Hirvonen, M. and S. A. Tretyakov, "Near-zero permittivity substrates for horizontal antennas: Performance enhancement and limitations," *Microwave and Optical Technology Letters*, Vol. 50, No. 10, 2008.

10. Ikonen, P. M. T., S. I. Maslovski, C. R. Simovski, and

S. A. Tretyakov, "On artificial magnetodielectric loading for improving the impedance bandwidth properties of microstrip antennas," *IEEE Transactions on Antennas and Propagation*, Vol. 54, 1654–1662, 2006.

11. Li, R. L., G. DeJean, M. M. Tentzeris, J. Papapolymerou, and J. Laskar, "Radiation-pattern improvement of patch antennas on a large-size substrate using a compact soft-surface structure and its realization on LTCC multilayer technology," *IEEE Transactions on Antennas and Propagation*, Vol. 53, No. 1, 200–208, 2005.

12. Nicholson, A. M. and G. F. Ross, "Measurement of the intrinsic properties of materials by time domain techniques," *IEEE Transactions on Instrumentation and Measurement*, Vol. 19, No. 4, 377–382, 1970.

13. Weir, W. B., "Automatic measurement of complex dielectric constant and permeability at microwave frequencies," *Proc. IEEE*, Vol. 62, 33–36, 1974.

14. Zhang, B., Y. Feng, J. Xiong, Y. Yang, and H. Lu, "Microwave-absorbing properties of de-aggregated flake-shaped carbonyl-iron particle composites at 2–18 GHz," *IEEE Transactions on Magnetics*, Vol. 42, No. 7, 1778–1881, 2006.

15. Folgueras, L., M. Alves, and M. Rezende, "Microwave absorbing paints and sheets based on carbonyl iron and polyaniline: Measurement and simulation of their properties," *Journal of Aerospace and Management*, Vol. 2, No. 1, 63–70, 2010.

16. Kuo, S.-K., S.-L. Chen, and C.-T. Lin, "An accurate method for impedance measurement of rfid tag antenna," *Progress In Electromagnetics Research*, Vol. 83, 93–106, 2008.

17. Kuo, S.-K. and L.-G. Liao, "An analytic model for impedance calculation of an RFID metal tag," to appear in *IEEE Antennas and Wireless Progagation Letters*.

18. Yang, G. M., X. Xing, A. Daigle, M. Liu, O. Obi, S. Stoute, K. Naishadham, and N. X. Sun, "Tunable miniaturized patch antennas with self-biased multilayer magnetic films," *IEEE Transactions on Antennas and Propagation*, Vol. 57, 2190–2193, 2009.

19. Yang, G. M., X. Xing, A. Daigle, O. Obi, M. Liu, S. Stoute, K. Naishadham, and N. X. Sun, "Loading effects of self-biased magnetic films on patch antennas with substrate/superstrate sandwich structure," *IEEE Transactions on Antennas and Propagation*, Vol. 58, 648–655, 2010.